Impact of Lanthanum-Doping on the Physical and Electrical Properties of Cobalt Ferrites

Asma Aslam[1] · Abdul Razzaq[1] · S. Naz[2] · Nasir Amin[1] · Muhammad Imran Arshad[1] · M. Ajaz Un Nabi[1] · Abid Nawaz[1] · Khalid Mahmood[1] · Aisha Bibi[3] · Faisal Iqbal[4] · M. Shakil[5] · Zahid Farooq[6] · Muhammad Zahir Iqbal[7] · Syed Shabhi Haider[7] · Atta ur Rehman[1]

Abstract
Cobalt ferrites have attracted extraordinary attention due to their high coercivity, chemical stability, and mechanical hardness. Lanthanum doped-cobalt ferrites having chemical formula $CoLa_xFe_{2-x}O_4$ with composition x = (0.00, 0.015, 0.045, 0.060) were synthesized by chemical co-precipitation method. The prepared samples were characterized by X-ray diffraction (XRD), Fourier-transform infrared spectroscopy (FTIR), Raman spectroscopy, and current-voltage (I-V) technique. The structure of the crystal was analyzed by X-ray diffraction. The crystallite size of nanoparticles was examined in the range of 21–25 nm, and a fluctuating trend was found with the inclusion of La^{3+} cations. The X-ray diffraction patterns verify the contraction of lattice constant and unit cell volume with the substitution of La^{3+} cations except for the concentration of x = 0.060. Lattice constant was in the range of 8.34 Å–8.41 Å while unit volume cell was in the range of 580 $Å^3$–596 $Å^3$. The resistivity of all samples was calculated by the application of two probes I-V technique. The maximum resistivity of the order of 81.129×10^5 Ω cm was found for the concentration of x = 0.060 at 723 K which makes it useful for high-frequency gimmicks applications. The resistivity and drift mobility were found inversely related to each other. The inverse relation low-frequency absorption band and high-frequency absorption bands were analyzed by Fourier-transform infrared spectroscopy technique.

1 Introduction

Electrical, dielectric, and structural properties of cobalt ferrites play an important role to design electronic, magnetic, and electrochemical devices. Spinel ferrites have practical applications in information storage systems, ferrofluid technology, magneto-caloric refrigeration, and magnetic diagnostics. The spinel ferrites represent an important class of ferromagnetic oxides due to their versatile electrical properties. Ferrites are those materials which are mostly used in modern technology. Due to chemical, electrical, magnetic, and physical characteristics, the researchers paid a special interest in these materials [1–4]. Ferrites have magnetized domains and also hysteresis and magnetic saturation. Ferrites show the paramagnetic behavior at a critical temperature; that temperature is called Curie temperature (Tc). Ferrites have magnetic properties that depend upon the chemical composition [5]. Ferrites have unique properties. Ferrites can be synthesized by different methods. Ferrites have two types; one is called soft ferrites that have low coercivity, and the other is called hard ferrites

✉ Muhammad Imran Arshad
 miarshadgcuf@gmail.com

1 Department of Physics, Government College University, Faisalabad 38000, Pakistan

2 Department of Physics, Government College Women University Faisalabad, Faisalabad, Pakistan

3 Institute of Functional Nano & Soft Materials (FUNSOM), Soochow University, Suzhou 215123, Jiangsu, China

4 Department of Physics, The Islamia University of Bahawalpur, Bahawalpur, Pakistan

5 Department of Physics, University of Gujrat, Gujrat 50700, Pakistan

6 Department of Physics, University of Education Lahore Faisalabad Campus, Faisalabad, Pakistan

7 Nanotechnology Research Laboratory, Faculty of Engineering Sciences, GIK Institute of Engineering Sciences and Technology, Topi, Khyber Pakhtunkhwa 23640, Pakistan

with high coercivity. Ferrites are commonly used in magnetic recording media, microwave absorbent, and sensors [6]. Nano-particles are used as removable antimicrobial photocatalyst [7]. These magnetic materials have a range of magnetic and electrical properties widely useful in the applications of modern technology. Ferrites are better than other magnetic materials due to low eddy current loss at high electrical resistivity. Ferrites have the general formula MFe_2O_4 [8]. Spinel ferrites are the common ferrites and used in different devices due to chemical stability, low dielectric loss, high Curie temperature (Tc), high permeability, and high saturation magnetization [9]. Ferrites are semiconductors in nature with magnetic oxide materials that are used in magnetic materials due to low electrical conductivity [10]. Nano-particles have fascinating properties that are superior to those of bulk. Nano-particles are very attractive by their captivating size that depends upon the chemical, mechanical, thermal, magnetic, electronic, and optical properties. Due to chemical stability, mechanical hardness, high coercivity, and saturation, magnetization cobalt ferrites are determined contenders for high-density magnetic recording media. The low size distribution of spinel ferrites is very important due to magnetic and electrical properties and magnetocaloric refrigeration, ferrofluid technology, and broad practicable in the information storage system. Cobalt ferrites are the low cost, high performance for high-frequency applications magnetic materials [11]. The cobalt ferrites possess an inverse spinel structure [12–14]. Kumar et al. [11] obtained high DC resistivity of the order of $\sim 20.621 \times 10^6$ Ωcm for x = 0.1 lanthanum-doped cobalt ferrite synthesized by co-precipitation method at the room. The crystallite size of their synthesized $CoFe_2O_4$ was 49 nm. A reduction in particle size with a deep study of resistivity is still required for practical applications. R. S. Yadav et al. [15] reported the effect of lanthanum incorporation on structural and electrical properties of cobalt ferrite synthesized by starch-assisted sol-gel combustion method. The particle size of $CoFe_2O_4$ was 21 nm. They studied a decreasing trend in crystallite size with the substitution of lanthanum into cobalt ferrites. The presence of five Raman peaks confirms that single-phase cubic spinel ferrites were formed. Mariosi et al. [16] studied the environmental applications of lanthanum-doped cobalt ferrites fabricated via the sol-gel method. The

crystallite size and lattice constant were found to decrease with the substitution of lanthanum. The particle size was in the range between 4.9 and 6.6 nm. Raman spectra showed inverse spinel structure and degree of inversion increases with an increase in dopant rare earth lanthanum. Gul et al. [12] reported the structural and electrical characteristics of $CoFe_2O_4$ via the sol-gel approach. The calculated particle size was in the range of 18–23 nm. The crystallite size for $CoFe_2O_4$ was reported 23 nm and decreased with the content. High DC electrical resistivity of the order of 1.06×10^9 Ω cm at 373 K was achieved with the inclusion of aluminum at x = 0.50. Yadav et al. [17] examined the effect of grain size and structural changes on electrical properties of cobalt ferrites prepared by honey mediated sol-gel combustion method. The research group observed that the particle size increased as the annealing temperature increased. The group obtained the crystallite size of 75 nm at annealing temperature of 900 °C. The research group noticed the presence of tetrahedral and octahedral sites in the fabricated cobalt ferrite by employing Raman and FTIR spectroscopy.

Amin et al. [18] studied the structural, electrical, optical, and dielectric properties of yttrium-doped cadmium ferrites and found the DC resistivity of soft-ferrites to be increased from 1.047×108–4.822×1010 Ω -cm at 523 K. this material was useful for high-frequency devices. Hussain et al. [19] fabricated cerium substituted Cu-Cd-Co ferrites and found it useful for transformers. Rehman et al. [20] prepared lanthanum-doped Zn-Co-Cu ferrites powder and found it useful in X-band microwave applications.

Nanomaterials with applications like microwave absorption and electromagnetic shielding [21, 22], excellent anode materials for lithium-ion battery, and photolysis catalysts [23], improved thermoelectric performance [24], and electrocatalyst [25, 26] have been fabricated by researchers.

Our research group feels that the formerly probing [11–17] on electrical features of lanthanum-doped cobalt ferrites has not been sufficiently investigated in detail especially the effect of temperature on resistivity for doping of small concentration of lanthanum in cobalt ferrites. In most of the research papers, the resistivity either increases or decreases with an increase or decrease in temperature, but in our research the resistivity has a peculiar behavior; first it increases with temperature, and

Table 1 XRD parameters of $CoLa_xFe_{2-x}O_4$ with composition (x = 0.00, 0.015, 0.045, 0.060)

Composition (x)	θ (degree)	(hkl)	Intensity	Crystallite size (nm)	Lattice constant (Å)	Unit cell volume ($Å^3$)	X-ray density (gcm^{-3})
0.00	17.831	(311)	287	21.73	8.3401	580.125	5.377
0.015	17.722	(311)	286	25.15	8.3896	590.509	5.306
0.045	17.661	(311)	284	21.17	8.4176	596.445	5.309
0.060	17.73	(311)	318	24.75	8.3868	589.928	5.395

Table 2 Raman active modes for as-prepared samples

Sample	Raman active mode positions (cm^{-1})				
	E_g	$T_{2g}(2)$	$T_{2g}(3)$	$T_{2g}(2)$	$A_{1g}(1)$
$CoFe_2O_4$	318.3	357.9	492.6	-	652.5
$CoLa_{0.015}Fe_{1.985}O_4$	301.0	363.2	484.0	-	653.8
$CoLa_{0.045}Fe_{1.95}O_4$	318.7	359.9	499.5	539.4	650.7
$CoLa_{0.060}La_{1.94}O_4$	325.9	363.9	495.8	537.2	652.3

then after a certain temperature, it starts decreasing so it possesses both the ferromagnetic and paramagnetic nature which was not discussed and shown in the literature study.

This research is an extension of the previously done researches on electrical properties of lanthanum-doped cobalt ferrites. One of the major reasons for this extension is that the past studies were not sufficient enough to deal with the said problem. Therefore, the researcher's group after finding the gap in the previous studies tried to successfully fill it out.

In this research work, the nanoparticles of lanthanum-doped cobalt ferrites were prepared using the co-precipitation method. The fabricated nanoparticles at a very small concentration of x = 0.060 exhibit a very high resistivity of the order of 52.594×10^8 Ω cm. So, this fabricated material may be a better choice for specified applications in high-frequency gimmicks.

2 Experiment and Characterizations

2.1 Synthesis

Co-precipitation method was used for the preparation of $CoLaxFe2-xO4$ with composition (x = 0.00, 0.015, 0.045, 0.060) using Co $(NO_3)_2.6H_2O$, La $(NO_3)_3.6H_2O$, and $FeCl_3.6H_2O$ as starting chemicals. The measured nitrates were put into different beakers and mixed up with de-ionized water for making a solution. The beakers were placed on a magnetic stirrer, and drops of NaOH solution were added to increase the pH of the solution up to 10. The stirring process of the solution continued for 30–40 min. The beakers were put in a water bath for 24 h at 95 °C. After that, the precipitates were washed with de-ionized water and ethanol and filtered. The filtrate was dried in an oven for 72 h. After that, each sample was ground. After grinding the substance was placed in a furnace and sintered at 900°C for 8 h. These samples were sintered and were subsequently cooled to ambient temperature.

2.2 Characterization Used

To record the diffraction peaks, the X-ray diffractometer (Bruker D8 Advance) with $\lambda = 0.154$ nm and 2θ range of 20º–60º was used. FTIR spectroscopy (Perkin) was employed to confirm absorption band spectra within the range of wave number 3000–400 cm^{-1}. Raman spectra were recorded using the LABRAM-HR commercial spectrometer. The DC resistivity was determined by the I-V measurement technique (Keithley Electrometer Model 2400).

3 Results and Discussion

3.1 XRD Study

The diffraction pattern of as-prepared samples as shown in Fig. 1(a) that exhibits all the characteristic peaks (220), (311), (222), (400), (422), and (511) of spinel cubic structure belongs to space group Fd-3 m [20] and Fig. 1(b) shows peak (311) shift towards smaller angle. It may be due to the substitution of greater radii La^{3+} cations to smaller radii cations Fe^{3+} [20]. XRD patterns (Fig. 1(a)) exhibit no secondary phases, so it verified the formation of a single-phase cubic structure of

Fig. 1 (a) XRD pattern and (b) Peak (311) shift of $CoLa_xFe_{2-x}O_4$ (x = 0.00, 0.015, 0.045, 0.060)
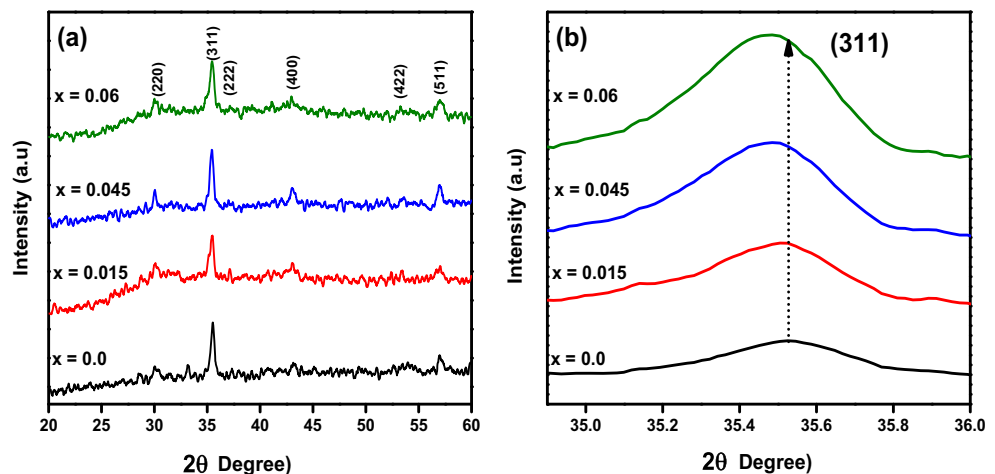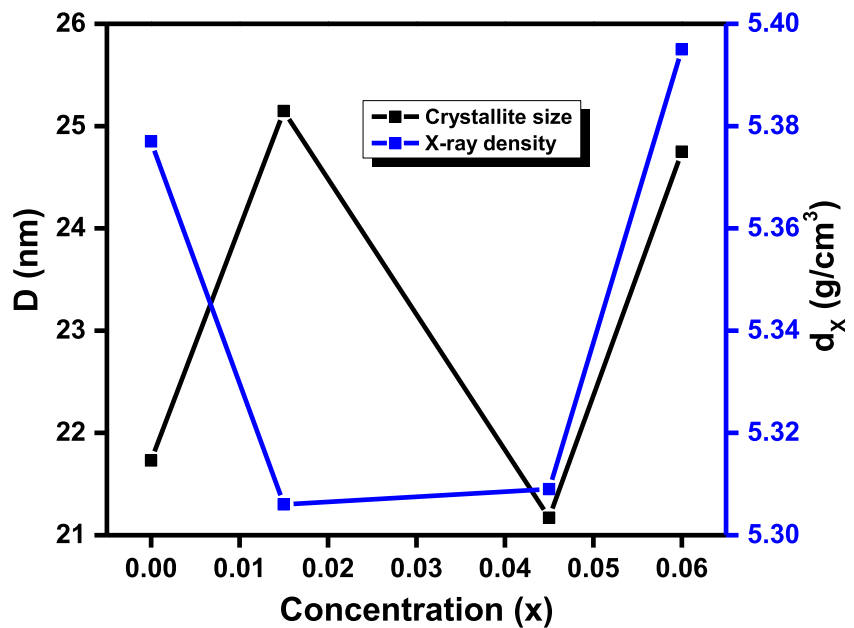
Fig. 2 A plot of concentration vs crystallite size and X-ray density of as-prepared samples

lanthanum-doped cobalt spinel ferrites. The crystallite size (D) of samples for the high-intensity peak (311) was calculated by using Scherer's formula given in Eq. (1) [27]:

$$D = \frac{0.9\lambda}{\beta\cos\theta} \tag{1}$$

where $\lambda = 1.5418$ Å is the wavelength of radiations and β is called the full-wave width at half maximum and θ belongs to Bragg's angle of diffraction. The crystallite size (D) for the compositions x = 0.00, 0.015, 0.045, and 0.060 are given in Table 1 and graphically as shown in Fig. 2 [15]. The maximum crystallite size was 25.147 nm, and the minimum value was 25.15 nm observed at x = 0.06 and

0.015, respectively, and as reported in the literature [28]. The lattice constant (a) of the as-prepared material was calculated through Eq. (2) [29]:

$$1/d^2 = \left(h^2 + k^2 + 1^2\right)/a \tag{2}$$

where hkl represents miller indices of the plane and "d" is known as d-spacing. The maximum value of lattice constant (a) was 8.41 Å at x = 0.045. It was observed that the lattice constant value increased from concentration x = 0.015 to x = 0.045, as reported in literature [30] and then decreased at x = 0.060. The variation of lattice constant with lanthanum listed in Table 2 shows an increasing trend with the substitution of lanthanum which may be attributed to the inclusion of lanthanum
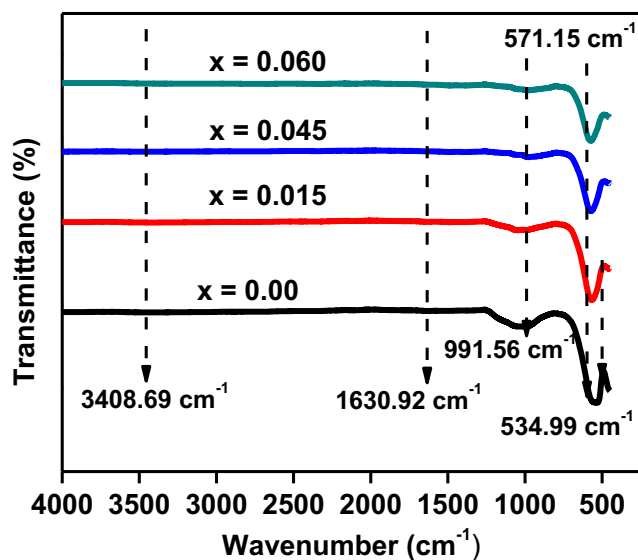

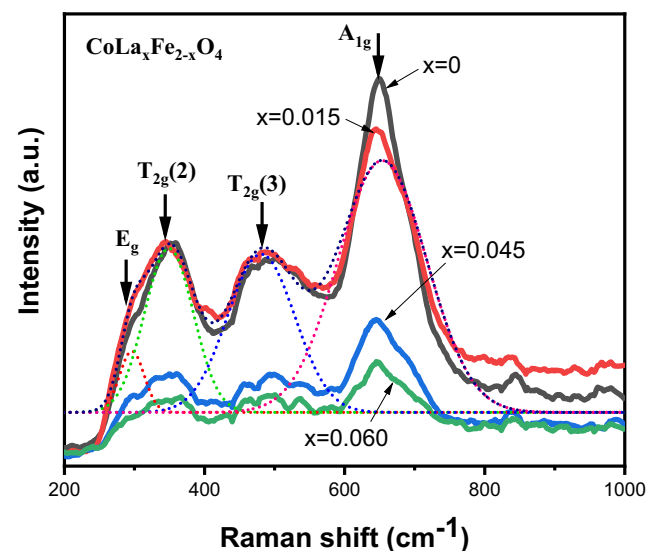**Fig. 3** FTIR spectra of CoLa$_x$Fe$_{2-x}$O$_4$ with composition (x = 0.00, 0.015, 0.045, 0.060)

Fig. 4 Raman graphs of CoLa$_x$Fe$_{2-x}$O$_4$ with composition (x = 0.00, 0.015, 0.045, 0.060)

Table 3 Resistivity of CoLaxFe$_{2-x}$O$_4$ (x = 0.00, 0.015, 0.045, 0.060) at different temperatures

Temperature (K)	Resistivity ×10^8 (ohm cm)			
	CoFe$_2$O$_4$	CoLa$_{0.015}$Fe$_{1.985}$O$_4$	CoLa$_{0.045}$Fe$_{1.955}$O$_4$	CoLa$_{0.060}$La$_{1.94}$O$_4$
303	0.780	8.571	0.392	52.594
423	8.377	17.151	0.152	36.250
523	0.355	0.790	0.008	4.165
623	0.029	0.054	0.0008	0.566
723	0.004	0.008	0.0001	0.081

La^{3+} cation which has a larger ionic radius (1.061 Å) in place of Fe^{3+} ions having a smaller ionic radius (0.67 Å) [31]. The unit cell volume (V) of the as-prepared material was calculated using the formula of Eq. (3) [9]:

$$V = a^3 \tag{3}$$

It was observed that with the addition of lanthanum cations, the values of unit cell volume of the material were changed. The value of unit cell volume rapidly increased by doping lanthanum at x = 0.015 to 0045 but decreased as lattice constant decreased at x = 0.060 given in Table 2. The unit cell volume observed was in the range of 580.125 Å^3–596.444 Å^3.

The X-ray density (d$_X$) of all samples was calculated by using the relation (4) [32, 33]:

$$d_X = \frac{ZM}{NV} \tag{4}$$

In the above equation, Z = 8 shows the number of molecules in the unit cell volume of spinel lattice. The calculated value of X-ray density is reported in Table 1 and graphically
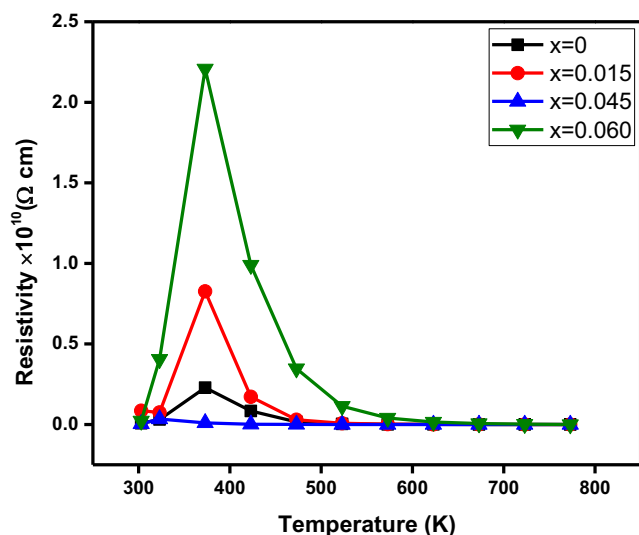

Fig. 5 A plot of DC electrical resistivity as a function of temperature of CoLa$_x$Fe$_{2-x}$O$_4$ (x = 0.00, 0.015, 0.045, 0.060)

represented in Fig. 2. The range of X-ray density of as-prepared material was 5.306 gcm^{-3}-5.395 gcm^{-3}.

3.2 FTIR Analysis

Figure 3 showed the FTIR spectrum of CoLa$_x$Fe$_{2-x}$O$_4$ with composition x = 0.00, 0.015, 0.045, and 0.060 nanocrystalline samples with the enhancement of lanthanum. Two fundamental absorption bands are shown by the spectra which are associated with the normal and inverse cubic spinel structure. The range of 500–600 cm^{-1} shows the higher frequency band which represents the vibrations of the tetrahedral group. The range of 300–490 cm^{-1} depicts the lower-frequency bands associated with vibrations of the octahedral group [34, 35]. The absorption band appearing at wavenumber 571.15 cm^{-1} is accredited to the metal-oxygen stretching vibration of Fe^{3+}-O$_2$. Another absorption band was observed at 991.56 cm^{-1} that represented the RCH=CH$_2$ alkene group [28]. The next band was observed at 1630.92 cm^{-1} which depicts the NO^{3-} stretching. In these, all sample broadband was observed in hydrogen-oxygen bonded O-H stretching vibration. The O-H stretching vibration in all samples showed the presence of adsorbed water in the material [28].

3.3 Raman Spectra Analysis

Raman spectroscopy is a powerful tool for investigating the lattice effects due to vibrational modes [16, 17]. Five active modes A_{1g}, E_g and three T_{2g} are seen in spinel group [36]. Here A, E, and T depict 1D (dimensional), 2D (dimensional), and 3D (dimensional), respectively. The movement of O^{2-} anions and cations at tetrahedral as well as at octahedral sites in spinel ferrites is correlated with these five Raman modes. The A_{1g} Raman mode exhibits the motion of O^{2-} anion and the residual four Raman modes E_g and three T_{2g} are associated with the motion of both O^{2-} and cations [15]. The inverse spinel structure of lanthanum-doped cobalt ferrites was investigated via Raman spectroscopy. All the samples show a spinel structure from Raman spectra. Raman spectra of sample CoFe$_2$O$_4$ shown in Fig. 4 depicts E_g, T_{2g}(2), T_{2g}(3), and A_{1g}
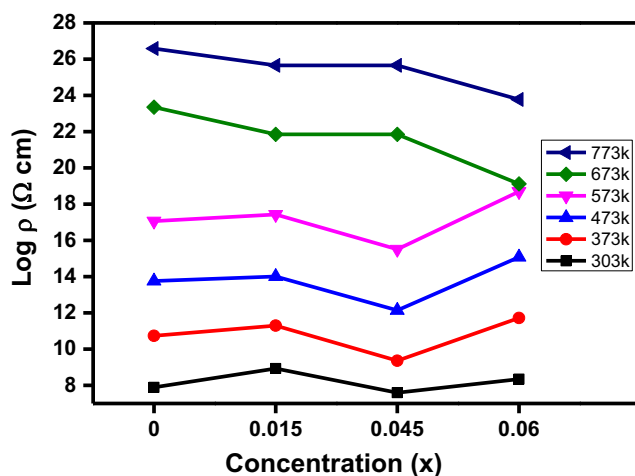
Table 4 DC electrical resistivity (ρ_{DC}), charge carrier concentration (η), drift mobility (μ_d), curie temperature (T_C), and activation energy (E_p, E_f and ΔE) of $CoLa_xFe_{2-x}O_4$ (x = 0.00, 0.015, 0.045, 0.060)

Composition (x)	$\rho_{DC} \times 10^5 (\Omega\text{-cm})$ at 723 K	$\eta \times 10^{22}$	$\mu_d \times 10^{-10} (cm^2/\text{V-s})$ At 723 K	Curie temperature T_c (K)	Activation energy		$\Delta E = E_p - E_f$ (eV)
					E_p(eV)	E_f(eV)	
0.00	3.982	1.766	8.889	373	0.616	0.461	0.155
0.015	8.044	1.895	8.281	373	0.632	0.342	0.291
0.045	0.157	1.679	237.008	323	0.587	0.067	0.520
0.060	81.129	3.316	0.232	373	0.772	0.597	0.175

modes at 318.3 cm^{-1}, 357.9 cm^{-1}, 492.6 cm^{-1}, and 652.5 cm^{-1}, respectively, where T_{2g} corresponds to the vibrational mode of the octahedral site while A_{1g} mode corresponds to vibrational mode of tetrahedral site. The modes at 492.6 cm^{-1} is related to octahedral iron, and mode at 652.5 cm^{-1} is related to tetrahedral cobalt [16]. With the incorporation of lanthanum into cobalt ferrite, the Raman modes are shown in deconvoluted Fig. 4. The powerful Raman mode about 650.7 cm^{-1} matches A_{1g} and can be assigned to symmetric stretching of O^{2-} atoms along with Fe-O bonds at tetrahedral sites. The Raman mode $T_{2g}(3)$ about 484.0 cm^{-1} matches asymmetric bending of O^{2-} and the Raman modes $T_{2g}(2)$ about 357.9 cm^{-1} relate to asymmetric stretching of Me-O (Metal-Oxygen) and Fe-O at the octahedral site given in Table 2. The Raman mode E_g about 301.0 cm^{-1} can be assigned to symmetric bending of O^{2-} relative to metal ion [15]. The Raman peak position and Raman intensity both change which is owed to cation redistribution and crystallite size of $CoLa_xFe_{2-x}O_4$ with composition x = 0.00, 0.015, 0.045, and 0.060 nanoparticles.

3.4 I-V Measurements

The I-V measurements values for the synthesized samples were calculated in the temperature range of 303 K to 773 K while the temperature was changed in the steps of 50 K. For

the calculation of resistivity, the formulae used are given by eqs. (5) and (6) [32];

$$R = \frac{\rho L}{A} \tag{5}$$

$$\rho = RA/L \tag{6}$$

In the above eq. R is called resistance of the samples, '$A = \pi r^2$' is known as the area of the pallets, 'l' represent the thickness of pallets and 'ρ' is the resistivity of samples.

3.4.1 DC Electrical Resistivity as a Function of Temperature

Figure 5 shows the variations of resistivity with the increasing temperature. It is clear from Fig. 5 that every plot of each sample represents a certain temperature called Curie temperature (T_C); before this temperature the resistivity increases with the increase in temperature and after this temperature, and a decreasing trend of resistivity is found with the enhancing temperature. This may be associated with the drift mobility of the electric charge carriers because increasing temperature activates the electric charge carriers. The calculated values of resistivity for different concentrations of
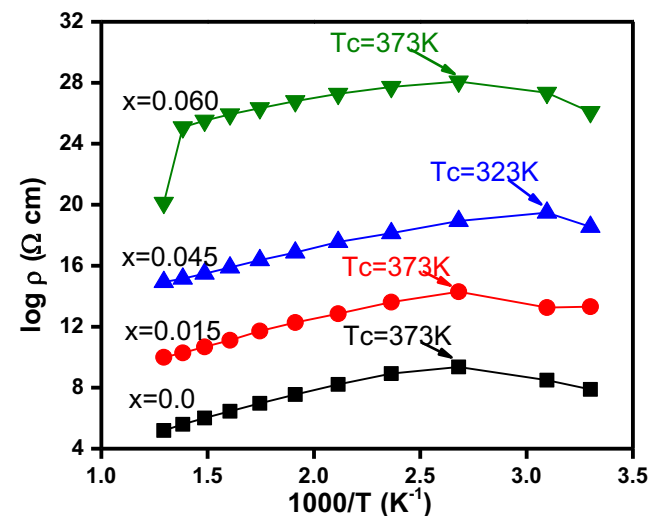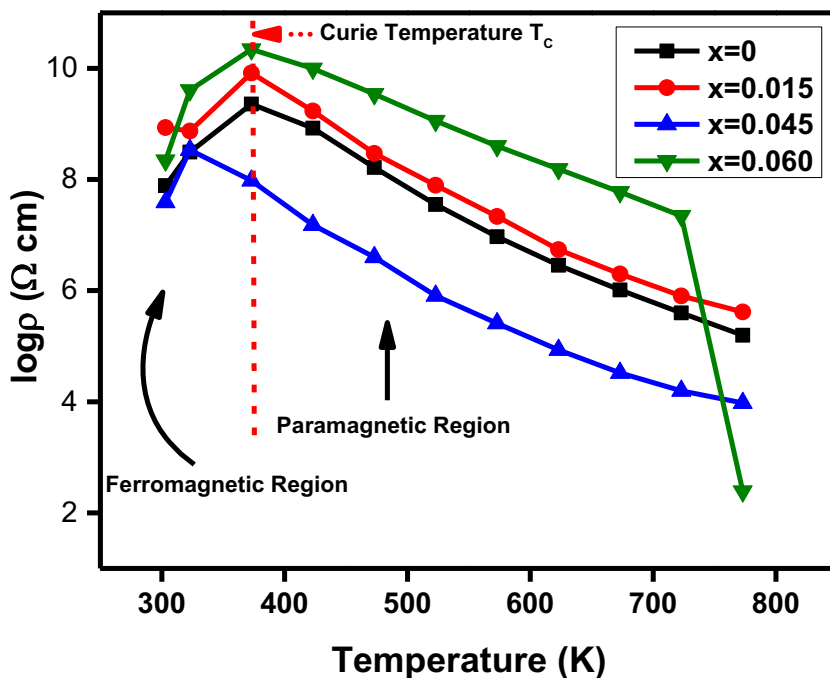
Fig. 6 A plot of resistivity vs concentration $CoLa_xFe_{2-x}O_4$ (x = 0.00, 0.015, 0.045, 0.060)

Fig. 7 A plot of DC electrical resistivity vs 1000/T of $CoLa_xFe_{2-x}O_4$ with composition x = (0.00, 0.015, 0.045, 0.060)

Fig. 8 Graph of DC electrical resistivity vs temperature of $CoLa_xFe_{2-x}O_4$ with composition (x = 0.00, 0.015, 0.045, 0.060) calcined at 1173 K for 8 h

lanthanum-doped cobalt ferrite nanoparticles at peculiar temperatures 303 K (room temperature), 423 K, 523 K, 623 K, and 723 K are given in Table 3. It is evident from Table 3 that the resistivity at room temperature is very high (0.780×10^8 Ω-cm at 303 K for pure $CoFe_2O_4$), and it first increases up to a specific temperature and then starts diminishing with the further increase in temperature (0.004×10^8 Ω-cm at 723 K for pure $CoFe_2O_4$). With the inclusion of lanthanum from x = 0 to x = 0.015 into the cobalt ferrites, the resistivity increases from 0.780×10^8 Ω cm at 303 K to 8.571×10^8 Ω cm at the same temperature, but the trend remains the same for the increasing temperature as for pure cobalt ferrites as can be seen from Table 3.
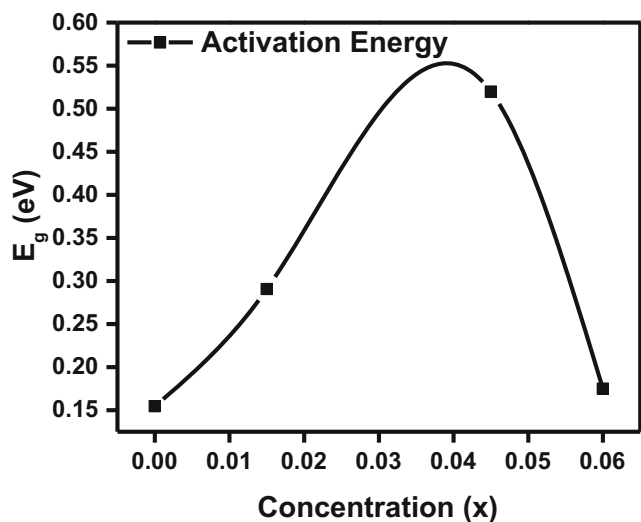
3.4.2 DC Resistivity as a Function of Lanthanum Composition

The conductivity of ferrites is attributed to the hopping mechanism of electrons. The hopping of electrons takes place between Me^{3+} (metal cations) and Fe^{3+} ions at different lattice sites [37, 38]. Hopping conductivity depends upon the two main factors (i) the distance between the centers of two adjacent octahedral sites (ii) repulsive force faced by hopping electrons present due to the negative charge on the activated electron and adjacent O^{2-} anions [37]. The conductivity of ferrites is significantly dependent on the presence of these divalent and trivalent ions in the octahedral sites [37]. Figure 6 exhibits an increasing trend in the resistivity of the nano ferrite system with the inclusion of lanthanum. When lanthanum is substituted into the
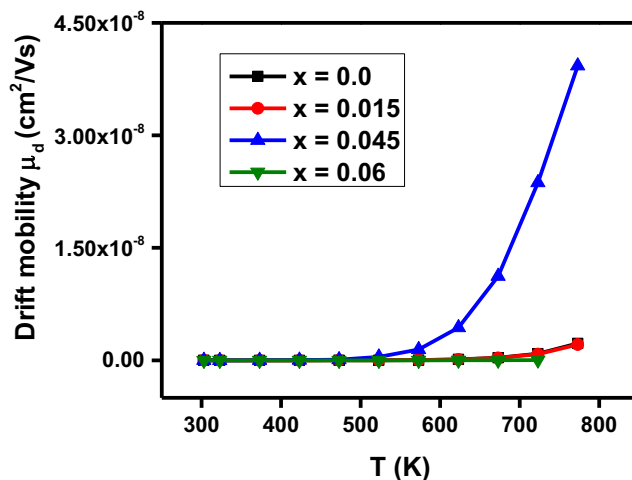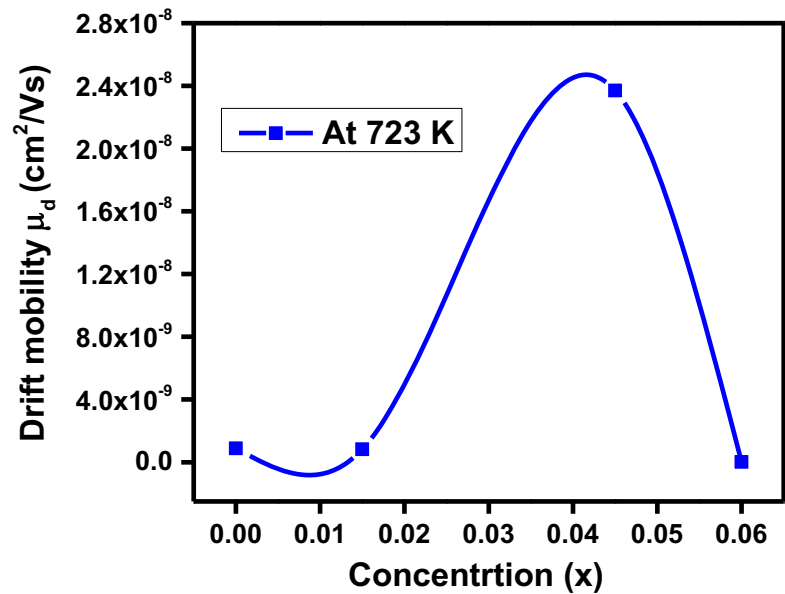

Fig. 9 Plot of activation energy vs concentration of $CoLa_xFe_{2-x}O_4$ (x = 0.00, 0.015, 0.045, 0.060)

Fig. 10 Plots of variation of drift mobility as a function of temperature of $CoLa_xFe_{2-x}O_4$ (x = 0.00, 0.015, 0.045, 0.060)

Fig. 11 A plot of variation of drift mobility as a function of composition of $CoLa_xFe_{2-x}O_4$ (x = 0.00, 0.015, 0.045, 0.060)

cobalt ferrites, it preferred to occupy the octahedral (B) sites; due to this reason, ferric Fe^{3+} ions were forced to migrate to tetrahedral (A) sites and as a result conductivity decreased. As more contents of lanthanum cations x = 0.060 were substituted, more Fe^{3+} ions migrated to tetrahedral sites, and consequently, Verwey's hopping mechanism is blocked and resistivity increased. The same increasing trend of resistivity was reported by Kumar et al. [11]. The DC electrical resistivity increased for samples $CoLa_{0.015}Fe_{1.985}O_4$ and $CoLa_{0.060}La_{1.94}O_4$ and is tabulated in Table 4.

3.4.3 Activation Energy

The Arrhenius plots (log of DC electrical resistivity versus 1000/T) for different compositions of as-prepared nanoferrite system were represented in Fig. 7. Activation energies of hopping electrons were calculated from the slopes of Arrhenius plots using the formula [39]:

$$E_a = 2.303 \times k_B \times 10^3 \times solpe \text{ (eV)} \qquad (7)$$

where $k_B = 8.602 \times 10^{-5} eV/K$ is called Boltzmann constant. Figure 7 represents an alteration in the slope at a certain temperature of resistivity curves of all the Co-La nanoferrite system. This peculiar temperature called the Curie temperature (T_c) splits the resistivity curve into two regions following ferrimagnetic and paramagnetic regions due to change in magnetic ordering as shown by Fig. 8. It can be seen from Fig. 8 that the region below the curie temperature is designated as a ferromagnetic region while the region above the curie temperature is the paramagnetic region. The calculated values of activation energies for both ferromagnetic and paramagnetic regions for all the compositions are shown in Table 4. The higher values of activation energies for the paramagnetic

region as compared with the ferromagnetic region for all the compositions as shown by Table 4 confirm the theory of Irkhin and Turov [40] which is owed to the fact that magnetic domains in ferromagnetic material are more ordered than in paramagnetic [41]. Thus, the change in magnetic ordering in the nanomaterials also controls the conduction in ferrites. Such results were also reported in Mg-Cr nano ferrites [39], Cu^{2+}-doped Zn-Co-Ce nanoferrites [41], and Ni-Al [42]. It was clear from Table 4 that the activation energy in the paramagnetic region varies between 0.587 eV and 0.772 eV. It was observed from Fig. 9 that the minimum activation energy was 0.155 eV for pure Co^{2+} nanoferrites. The fluctuations in activation energies are similar to that of resistivity with the substitution of lanthanum because activation energy is directly dependent on DC electrical resistivity [39].

3.4.4 Drift Mobility as a Function of Temperature and Composition

Drift mobility of samples was determined using Eq. (8) [43, 44]:

$$\mu_d = \frac{1}{\eta e \rho_{DC}} \qquad (8)$$

where ρ_{DC} represents the DC electrical resistivity, η is the charge carrier concentration, and e shows charge on hopping electron. The charge carrier concentration was evaluated employing relation (9) [41].

$$\eta = \frac{N_a \rho_s P_{Fe}}{M} \qquad (9)$$

Here N_a = Avogadro's number, ρ_s = sintered density, P_{Fe} = Number of atoms in the compositional formula, and M =

Molecular weight of synthesized samples. The relations (8) and (9) were employed for the calculation of values of drift mobility and electric charge carrier concentration for all the fabricated samples of lanthanum-doped cobalt ferrite. The values of drift mobility remained in the range of $237.008 \times 10^{-10} cm^2/V$-s and $0.232 \times 10^{-10} cm^2/V$-s at 723 K. It can be seen from Fig. 10 that drift mobility of synthesized material depends upon temperature. It is clear from Fig. 10 that drift mobility increases with the increase in temperature which may be due to the reason that the increasing temperature provides energy to the hopping electrons so they jump from one lattice site to the other, and resistivity of the Co-La system decreased while conductivity increased [45]. It was clear from Fig. 11 that the drift mobility for the sample $CoLa_{0.045}Fe_{1.955}O_4$ is maximum of the order of $237.008 \times 10^{-10} cm^2/V$-s at 273 K, while for the sample $CoLa_{0.060}La_{1.94}O_4$ is minimum $0.232 \times 10^{-10} cm^2/V$-s at 723 K.

4 Conclusion

The present study depicts the effect of lanthanum incorporation in cobalt ferrites on structural, optical, and electrical characteristics. The XRD analysis of lanthanum-incorporated cobalt ferrites shows a cubic inverse spinel structure of prepared nanomaterial. The crystallite size varied between 21.17 and 25.15 nm. The maximum value of the crystallite size was 25.15 nm for $CoLa_{0.015}Fe_{1.985}O_4$. The crystallite size varied randomly with the substitution of lanthanum. The resistivity of nanomaterial first increases with temperature showing conducting behavior and then started decreasing with further increase in temperature showing semiconducting behavior; however, this behavior change occurs at 373 K. The activation energy was also maximum for the sample $CoLa_{0.060}La_{1.94}O_4$. FTIR analysis of fabricated nanomaterial shows the change in intensity of frequencies due to the doping of lanthanum. Raman spectra show the redistribution of cations at tetrahedral and octahedral sites. The drift mobility was found dependent on temperature. Our research group was successfully in obtaining the optimized resistivity of the order of 52.594×10^8 Ωcm for the sample $CoLa_{0.060}La_{1.94}O_4$ at a much smaller concentration of lanthanum x = 0.060. So, for the manufacturing of intermediate and high-frequency electromagnetic absorbers and high-frequency gimmicks, our fabricated material can be preferred for the specified applications.

References

1. Wang, X., Li, Y., Li, J., Yu, G., Zuo, L., Zhang, H.: Effect of $BiVO_4$ doping on the magnetic properties and microstructure of NiCuZn ferrites. J. Mater. Sci. Mater. Electron. **25**(10), 4230–4234 (2014)

2. Yuan, L., Zhu, H., Jin, Y.: Microstructure and magnetic properties of low-temperature-fired NiCuZn ferrites with SiO_2–CaO–Na_2O–K_2O glass. J. Mater. Sci. Mater. Electron. **27**(1), 198–202 (2016)

3. Huan, L., Tang, X., Su, H., Zhang, H., Jing, Y.: Effects of SiO_2 concentration on the DC-bias-superposition characteristics of the NiCuZn ferrites. J. Mater. Sci. Mater. Electron. **26**(5), 3275–3281 (2015)

4. Jin, Y., Zhu, H., Xu, Y., Zhu, H., Zhou, H., Jin, Y.: Microstructure and magnetic properties of low-temperature-fired NiCuZn ferrites with various borosilicate glasses. J. Mater. Sci. Mater. Electron. **27**(1), 517–521 (2016)

5. Zahir, R., Chowdhury, F.-U.-Z., Uddin, M., Hakim, M.: Structural, magnetic and electrical characterization of cd-substituted mg ferrites synthesized by double sintering technique. J. Magn. Magn. Mater. **410**, 55–62 (2016)

6. Singh, S., Sahai, A., Katyal, S., Goswami, N.J.M.S.-P.: Structural, optical and vibrational study of zinc copper ferrite nanocomposite prepared by exploding wire technique. Mater. Sci.-Pol. **36**(4), 722–732 (2018)

7. Yang, Y., Wang, F., Shao, J., Huang, D., Wan, M., Cao, Q.: Effects of La/Zn ratios on structural and magnetic properties of $Sr_{1-x}La_xFe_{12-y}Zn_yO_{19}$ hexagonal ferrites. Mater. Technol. **32**(3), 165–170 (2017)

8. Arshad, M., Maqsood, A., Gul, I., Anis-Ur-Rehman, M.: Fabrication, electrical and dielectric characterization of Cd-Ni nanoferrites. Mater. Res. Bull. **87**, 177–185 (2017)

9. Wang, Y., Wu, X., Zhang, W., Chen, W.: Synthesis and electromagnetic properties of La-doped Ni–Zn ferrites. J. Magn. Magn. Mater. **398**, 90–95 (2016)

10. Al Angari, Y.: Magnetic properties of La-substituted NiFe2O4 via egg-white precursor route. J. Magn. Magn. Mater. **323**(14), 1835–1839 (2011)

11. Kumar, P., Sharma, S., Knobel, M., Singh, M.: Effect of La^{3+} doping on the electric, dielectric and magnetic properties of cobalt ferrite processed by co-precipitation technique. J. Alloys Compd. **508**(1), 115–118 (2010)

12. Gul, I., Maqsood, A.: Structural, magnetic and electrical properties of cobalt ferrites prepared by the sol–gel route. J. Alloys Compd. **465**(1–2), 227–231 (2008)

13. Mane, D., Devatwal, U., Jadhav, K.J.M.L.: Structural and magnetic properties of aluminium and chromium co-substituted cobalt ferrite. Mater. Lett. **44**(2), 91–95 (2000)

14. Sawatzky, G., Van Der Woude, F., Morrish, A.: Cation distributions in octahedral and tetrahedral sites of the ferrimagnetic spinel $CoFe_2O_4$. J. Appl. Phys. **39**(2), 1204–1205 (1968)

15. Yadav, R.S., et al.: Influence of La^{3+} on structural, magnetic, dielectric, electrical and modulus spectroscopic characteristics of single phase $CoFe_{2-x}La_xO_4$ nanoparticles. J. Mater. Sci. Mater. Electron. **28**(12), 9139–9154 (2017)

16. Mariosi, F.R., Venturini, J., da Cas Viegas, A., Bergmann, C.P.: Lanthanum-doped spinel cobalt ferrite ($CoFe_2O_4$) nanoparticles for environmental applications. Ceram. Int. **46**(3), 2772–2779 (2020)

17. Yadav, R.S., et al.: Impact of grain size and structural changes on magnetic, dielectric, electrical, impedance and modulus spectroscopic characteristics of $CoFe_2O_4$ nanoparticles synthesized by honey mediated sol-gel combustion method. Adv. Nat. Sci. Nanosci. Nanotechnol. **8**(4), 045002 (2017)

18. Amin, N., et al.: Structural, electrical, optical and dielectric properties of yttrium substituted cadmium ferrites prepared by Co-Precipitation method. Ceram. Int. **46**, 20798–20809 (2020)

19. Hussain, K., Amin, N., Arshad, M.I.: Evaluation of structural, optical, dielectric, electrical, and magnetic properties of Ce^{3+} doped $Cu_{0.5}Cd_{0.25}Co_{0.25}Fe_{2-x}O_4$ spinel nano-ferrites. Ceram. Int. (2020). https://doi.org/10.1016/j.ceramint.2020.09.185

20. Rehman, A.U., et al.: Controllable synthesis of La^{3+} doped $Zn_{0.5}Co_{0.25}Cu_{0.25}Fe_{2-x}La_xO_4$ (x= 0.0, 0.0125, 0.025, 0.0375,

0.05) nano-ferrites by sol-gel auto-combustion route. Ceram. Int. **46**, 29297–29308 (2020)

21. Jian, X., et al.: Heterostructured nanorings of Fe− Fe_3O_4@ C hybrid with enhanced microwave absorption performance. ACS Appl. Mater. Interfaces. **10**(11), 9369–9378 (2018)

22. Jian, X., et al.: Facile synthesis of Fe_3O_4/GCs composites and their enhanced microwave absorption properties. ACS Appl. Mater. Interfaces. **8**(9), 6101–6109 (2016)

23. Jiang, J., Feng, Y., Mahmood, N., Liu, F., Hou, Y.: SnS_2/graphene composites: Excellent anode materials for lithium ion battery and photolysis catalysts. Sci. Adv. Mater. **5**(11), 1667–1675 (2013)

24. Farooq, M.U., et al.: Improved thermoelectric performance of BiCuSeO by Ag substitution at Cu site. J. Alloys Compd. **691**, 572–577 (2017)

25. Khan, M.W., et al.: Nitrogen-Doped Oxygenated Molybdenum Phosphide as an Efficient Electrocatalyst for Hydrogen Evolution in Alkaline Media. Front. Chem. **8**, 733 (2020)

26. Mohiuddin, M., et al.: Synthesis of two-dimensional hematite and iron phosphide for hydrogen evolution. J. Mater. Chem. A. **8**(5), 2789–2797 (2020)

27. Liu, Y., Wei, S., Xu, B., Wang, Y., Tian, H., Tong, H.: Effect of heat treatment on microwave absorption properties of Ni–Zn–Mg–La ferrite nanoparticles. J. Magn. Magn. Mater. **349**, 57–62 (2014)

28. Dasan, Y.K., Guan, B.H., Zahari, M.H., Chuan, L.K.: Influence of La^{3+} Substitution on Structure,Morphology and Magnetic Properties of Nanocrystalline Ni-Zn Ferrite. (2017). https://doi.org/10.1371/journal.pone.0170075

29. El-Hagary, M., Matar, A., Shaaban, E.R., Emam-Ismail, M.: The influence of cd doping on the microstructure and optical properties of nanocrystalline copper ferrite thin films. Mater. Res. Bull. **48**, 2279–2285 (2013)

30. Lin, Q., Yuan, G., He, Y., Wang, L., Dong, J., Yu, Y.: The influence of La-substituted Cu0.5Co0.5Fe2O4 nano particles on its structural and magnetic properties. Mater. Des. **78**, 80–84 (2015)

31. Demirci, Ç., Manna, P., Wroczynskyj, Y., Aktürk, S., Van Lierop, J.: Lanthanum ion substituted cobalt ferrite nanoparticles and their hyperthermia efficiency. J. Magn. Magn. Mater. **458**, 253–260 (2018)

32. Bhukal, S., Bansal, S., Singhal, S.: Co0.6Zn0.4Cu0.2CdxFe1.8−xO4 (0.2≤ x≤ 0.8) magnetic ferrite nano-particle: synthesis, characterization and photo-catalytic degradation of methyl orange. J. Mol. Struct. **1059**, 150–158 (2014)

33. Deepapriya, S., et al.: Investigation on lanthanum substitution in magnetic and structural properties of group IV elements. Vacuume. **161**, 5–13 (2019)

34. Masoudpanah, S., Ebrahimi, S.S., Derakhshani, M., Mirkazemi, S.: Structure and magnetic properties of La substituted $ZnFe_2O_4$ nanoparticles synthesized by sol–gel autocombustion method. J. Magn. Magn. Mater. **370**, 122–126 (2014)

35. Chaudhari, V., et al.: Crystallographic, magnetic and electrical properties of $Ni_{0.5}Cu_{0.25}Zn_{0.25}La_xFe_{2-x}O_4$ nanoparticles fabricated by sol–gel method. J. Alloys Compd. **549**, 213–220 (2013)

36. Wang, W., et al.: Microstructure and magnetic properties of MFe2O4 (M= Co, Ni, and Mn) ferrite nanocrystals prepared using colloid mill and hydrothermal method. J. Appl. Phys. **117**(17), 17A328 (2015)

37. Hosseinpour, A., Sadeghi, H., Morisako, A.: Simulation of DC-hopping conduction in spinel ferrites using free electron gas model. J. Magn. Magn. Mater. **316**(2), e283–e286 (2007)

38. Verwey, E., De Boer, F., Van Santen, J.H.: Cation arrangement in spinels. J. Chem. Phys. **16**(12), 1091–1092 (1948)

39. Raghasudha, M., Ravinder, D., Veerasomaiah, P.: Electrical resistivity studies of Cr doped mg nano-ferrites. Mater. Discov. **2**, 50–54 (2015)

40. Kharabe, R., Devan, R., Chougale, B.: Structural and electrical properties of cd-substituted Li–Ni ferrites. J. Alloys Compd. **463**(1–2), 67–72 (2008)

41. Hussain, K., et al.: Study of structural, optical, electrical and magnetic properties of Cu^{2+} doped $Zn_{0.4}Co_{0.6-x}Ce_{0.1}Fe_{1.9}O_4$ spinel ferrites. Phys. B Condens. Matter. **584**, 412078 (2020)

42. Patange, S., Shirsath, S.E., Lohar, K., Jadhav, S., Kulkarni, N., Jadhav, K.J.P.B.C.M.: Electrical and switching properties of $NiAl_xFe_{2-x}O_4$ ferrites synthesized by chemical method. Phys. B Condens. Matter. **406**(3), 663–668 (2011)

43. Hasolkar, S.S., Naik, P.: Effect of Gd^{3+} doping on structural, magnetic and electrical properties of $Mn_{0.5}Co_{0.5}Fe_{2-x}Gd_xO_4$ nanoparticles prepared using combustion synthesis. J. Alloys Compd. **823**, 153603 (2020)

44. Kamran, M., Anis-ur-Rehman, M.: Enhanced transport properties in Ce doped cobalt ferrites nanoparticles for resistive RAM applications. J. Alloys Compd. **822**, 153583 (2020)

45. Iqbal, M.J., Siddiquah, M.R.: Structural, electrical and magnetic properties of Zr–mg cobalt ferrite. J. Magn. Magn. Mater. **320**(6), 845–850 (2008)